Research Square

Preprints are preliminary reports that have not undergone peer review.
They should not be considered conclusive, used to inform clinical practice,
or referenced by the media as validated information.

# Stacking Sequence Optimization of Trapezoidal Hybrid Metal-Composite Swept Wings for Flutter Speed using EA-PSO Algorithm

**Hadi Ghashochi-Bargh**

ghashochi.b@bzte.ac.ir

Buein Zahra Technical University

**Salman Shafaghat**

Researcher at Malek Ashtar University of Technology

**Ali Dehghani-Ghobadi**

Amirkabir University of Technology

**Saeid Irani**

K.N. Toosi Univeristy of Technology

**Research Article**

**Keywords:** Flutter, Elitist adaptive particle swarm optimization, Stacking sequence optimization, Trapezoidal swept wing, Hybrid metal–composite structure

**Posted Date:** November 26th, 2026

**DOI:** https://doi.org/10.21203/rs.3.rs-11799583/v1

**License:** This work is licensed under a Creative Commons Attribution 4.0 International License.
Read Full License

**Additional Declarations:** No competing interests reported.

# Stacking Sequence Optimization of Trapezoidal Hybrid Metal-Composite Swept Wings for Flutter Speed using EA-PSO Algorithm

Hadi Ghashochi-Bargh[a], Salman Shafaghat[b], Ali Dehghani-Ghobadi[c], Saeid Irani[d]

[a] Department of Industrial, Mechanical and Aerospace Engineering, Buein Zahra Technical University, Buein Zahra, Iran.

[b] Researcher at Malek Ashtar University of Technology, Tehran, Iran.

[c] Faculty of Aerospace Engineering, Amirkabir University of Technology, Tehran, Iran.

[d] Faculty of Aerospace Engineering, K.N. Toosi Univeristy of Technology, Tehran, Iran.

**Abstract**

In the present work, the stacking sequence optimization of trapezoidal hybrid metal–composite swept wings for maximum flutter speed is investigated. For this purpose, the classical plate theory is used to model the structural behavior, the deflections are determined using the assumed-modes method, the aerodynamic forces are calculated using piston theory, and the flutter speed is computed with the p-method. The main contribution of this work is the use of an elitist adaptive particle swarm optimization (EA-PSO) algorithm with a new inertia-weight function. Its performance is first compared with that of the basic particle swarm optimization algorithm, which demonstrates the superior efficiency of the present algorithm. The EA-PSO algorithm is then applied to maximize the flutter speed of the hybrid wing, and the optimization results are presented for different metal span fractions, aspect ratios, taper ratios and sweep angles. The results show that increasing the metal span fraction, defined as the ratio of the metallic segment length to the semi-span, does not monotonically increase or decrease the maximum flutter speed. Instead, both the optimum metal span fraction and the corresponding maximum flutter speed differ from one geometry to another, which highlights the importance of treating the metal span fraction as a key design parameter in flutter optimization. Finally, the proposed inertia-weight function is shown to be effective and may be adopted in future studies.

**Keywords:**

Flutter; Elitist adaptive particle swarm optimization; Stacking sequence optimization; Trapezoidal swept wing; Hybrid metal–composite structure

## 1. Introduction

Several studies have addressed the flutter characteristics and aeroelastic optimization of laminated composite structures. Sawyer [1] investigated the supersonic flutter of laminated composite plates and examined the effects of ply number and orientation, lamina orthotropy, plate aspect ratio, in-plane loads, and cross-flow angle, including composite-stiffened aluminium plate designs. Weisshaar and Bohlmann [2] studied the aeroelastic tailoring of swept wings and demonstrated the significant influence of structural, aerodynamic, and inertial parameters on flutter stability. Cho and Chang [3] analyzed the supersonic flutter of a low-aspect-ratio wing using the panel method coupled with finite element structural modeling. Zhang et al. [4] compared different aerodynamic formulations for supersonic flutter analysis and showed that local piston theory provides improved accuracy over classical piston theory while requiring substantially lower computational effort than the unsteady Euler approach.

Golparvar et al. [5] investigated the flutter behavior of a cropped delta wing carrying an external store in subsonic incompressible flow. Their numerical predictions showed satisfactory agreement with experimental measurements, and the effects of the wing thickness, aspect ratio, store mass, and store center-of-gravity location on the flutter speed were quantified. Shokrollahi and Shafaghat [6] examined the supersonic flutter characteristics of a hybrid metal–composite wing using the Mach box method. Their parametric study demonstrated that the composite-to-metal ratio, sweep angle, taper ratio, and aspect ratio significantly affect the flutter behavior, and an optimal

composite-to-metal ratio was identified at which the flutter Mach number reaches its maximum value. Guo et al [7] performed the structural optimization of a swept composite wing with the objective of maximizing the flutter speed, using both gradient-based and genetic-algorithm approaches; comparable improvements in flutter performance were obtained with the two strategies. Song and Li [8] optimized the placement of piezoelectric actuators and sensors for the active suppression of supersonic flutter in laminated composite panels. Torabi and Afshari [9] employed particle swarm optimization to maximize the flutter speed of trapezoidal functionally graded plates and investigated the effects of the aspect ratio, plate thickness, core thickness, and fiber orientation. Guimarães et al. [10] conducted a multi-objective optimization of the flutter and buckling characteristics of laminated composite plates, considering the fiber orientation and boundary conditions as design variables. Qalandari et al. [11] developed a machine-learning-based framework for the aeroelastic optimization of a high-aspect-ratio wing equipped with an aileron. Their results indicated that the aileron location and mass properties significantly influence both the flutter speed and the flutter frequency, and an optimized configuration was obtained that delays the onset of flutter instability. Amozgar et al. [12] investigated the aeroelastic instability of a wing with an initial out-of-plane curvature and showed that the geometric curvature can considerably modify the flutter speed and frequency through changes in the interacting aeroelastic modes. Zafari et al. [13] investigated the nonlinear aeroelastic response and flutter sensitivity of a high-aspect-ratio wing subjected to a transverse follower force. Their sensitivity analysis revealed that the follower force, its spanwise location, and the structural and geometric properties of the wing influence the flutter margin, with the wing chord and the mass per unit length exhibiting particularly significant effects. Guo et al. [14] investigated the flutter characteristics of carbon-based nanohybrid composite panels using higher-order shear deformation and piston theories. The

accuracy of their formulation was validated by comparing the predicted natural frequencies and critical aerodynamic pressures with previously published results, which demonstrated its effectiveness for the flutter analysis of thick hybrid plates under different boundary conditions.

Collectively, these studies demonstrate that flutter stability is strongly governed by the structural configuration, geometric parameters, material distribution, fiber orientation, and aeroelastic coupling. Nevertheless, systematic investigations on the optimization of stacking sequences in trapezoidal hybrid metal–composite swept wings remain relatively limited. In particular, the combined effects of the stacking sequence and the wing geometric parameters on the flutter speed have not been sufficiently addressed. Therefore, the present study focuses on optimizing the stacking sequence of a trapezoidal hybrid metal–composite swept wing to maximize its flutter speed and enhance its aeroelastic stability.

In the present work, flutter optimization is carried out for trapezoidal hybrid wings, which are employed in modern supersonic aircraft and cruise missiles. Such wings consist of a metallic segment extending from the root over part of the span, and a composite segment extending from that station to the tip. This configuration is motivated by the loading conditions at the wing root: the maximum bending moment due to the inertial and aerodynamic loads occurs there, and these loads act in several directions. Since composite laminates provide high strength only along specific fiber directions and are comparatively weak at joints, a metallic root is preferred in the design of such wings. The outboard portion of the span is made of composite material in order to exploit its weight-saving advantage. This configuration is illustrated for a trapezoidal hybrid plate in Figure 1. On this basis, the flutter optimization of such wings is studied in the present work, and the effects of various geometric parameters — namely the metal span fraction, aspect ratio, taper ratio and sweep angle — are investigated using the elitist adaptive particle swarm optimization algorithm.

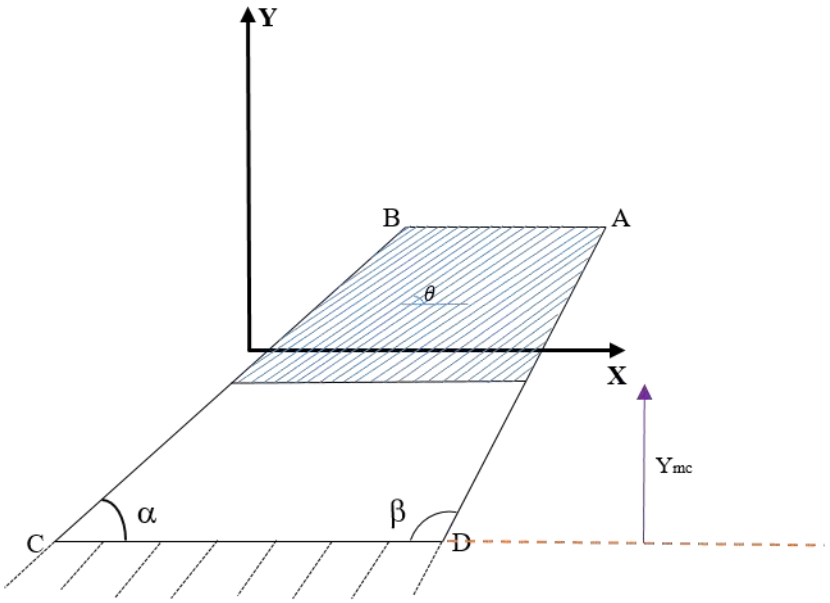



**Fig. 1.** A trapezoidal hybrid plate.

## 2. Aeroelasticity

In this section, the theoretical formulation of the flutter analysis of trapezoidal hybrid wings is presented, including the structural, aerodynamic, and aeroelastic modeling.

### 2.1 Structural Equations

The results presented in this paper are obtained for thin trapezoidal hybrid wings; therefore, the classical plate theory is adopted in the present analysis. Based on this theory, the displacement components of the plate along the $x, y$ and $z$ directions are expressed as follows:

$$u = \bar{u} - z\frac{\partial w}{\partial x},\ v = \bar{v} - z\frac{\partial w}{\partial y},\ w = \bar{w} \tag{1}$$

Assuming a linear strain–displacement relationship, there is no coupling between the in-plane and out-of-plane degrees of freedom. Consequently, the in-plane displacements of the mid-plane are neglected, that is, $\bar{u} = \bar{v} = 0$, and the displacement field reduces to:

$$\begin{cases} \varepsilon_{xx} = \dfrac{\partial u}{\partial x} = -\mathrm{z}\dfrac{\partial^2 w}{\partial x^2} \\ \varepsilon_{yy} = \dfrac{\partial v}{\partial y} = -\mathrm{z}\dfrac{\partial^2 w}{\partial y^2} \\ \varepsilon_{xy} = \dfrac{\partial u}{\partial y} + \dfrac{\partial v}{\partial x} = -2\mathrm{z}\dfrac{\partial^2 w}{\partial x \partial y} \end{cases} \tag{2}$$

The stress–strain relationship for a thin plate is also given by:

$$\begin{Bmatrix} \sigma_1 \\ \sigma_2 \\ \sigma_{12} \end{Bmatrix} = \begin{bmatrix} \dfrac{E}{\left(1-\nu^2\right)} & \dfrac{E\nu}{\left(1-\nu^2\right)} & 0 \\ \dfrac{E\nu}{\left(1-\nu^2\right)} & \dfrac{E}{\left(1-\nu^2\right)} & 0 \\ 0 & 0 & \dfrac{E}{2\left(1+\nu\right)} \end{bmatrix} \begin{Bmatrix} \varepsilon_1 \\ \varepsilon_2 \\ \varepsilon_{12} \end{Bmatrix} \tag{3}$$

where $E$ is the modulus of elasticity and $\nu$ is Poisson's ratio of the plate [15, 16].

In this research, the classical laminated plate theory (CLPT) is employed for thin laminated composite plates. This theory is analogous to the classical plate theory, except for the material properties and the stress–strain relations.

The stress–strain relationship based on the CLPT is presented in Equation (4) in the principal material axes of the lamina, where directions 1 and 2 denote the fiber direction and the direction perpendicular to it, respectively. In this equation, $E_1$ and $E_2$ are the moduli of elasticity along directions 1 and 2, $G_{12}$ is the shear modulus in the 1–2 plane, and $\nu_{12}$ and $\nu_{21}$ are the major and minor Poisson's ratios, respectively [17].

$$\begin{Bmatrix}\sigma_1\\ \sigma_2\\ \sigma_{12}\end{Bmatrix}=\begin{bmatrix}Q_{11} & Q_{12} & 0\\ Q_{21} & Q_{22} & 0\\ 0 & 0 & Q_{66}\end{bmatrix}\begin{Bmatrix}\varepsilon_1\\ \varepsilon_2\\ \varepsilon_{12}\end{Bmatrix}$$

$$Q_{11}=\frac{E_1}{(1-\nu_{12}\nu_{21})}, Q_{12}=Q_{21}=\frac{\nu_{12}E_2}{(1-\nu_{12}\nu_{21})}$$

$$Q_{22}=\frac{E_2}{(1-\nu_{12}\nu_{21})}, Q_{66}=G_{12}$$

(4)

Equation (4) represents Hooke's law for a lamina, expressed in the principal material axes (1–2) of the lamina. This relationship can be written in the global coordinate system ($x$, $y$) as follows:

$$\begin{Bmatrix}\sigma_x\\ \sigma_y\\ \sigma_{xy}\end{Bmatrix}=\begin{bmatrix}\bar{Q}_{11} & \bar{Q}_{12} & \bar{Q}_{16}\\ \bar{Q}_{12} & \bar{Q}_{22} & \bar{Q}_{26}\\ \bar{Q}_{16} & \bar{Q}_{26} & \bar{Q}_{66}\end{bmatrix}.\begin{Bmatrix}\varepsilon_x\\ \varepsilon_y\\ \varepsilon_{xy}\end{Bmatrix}$$

(5)

where

$$\bar{Q}_{11}=Q_{11}\cos^4\theta+2(Q_{12}+2Q_{66})\sin^2\theta\cos^2\theta+Q_{22}\sin^4\theta$$
$$\bar{Q}_{12}=(Q_{11}+Q_{22}-4Q_{66})\sin^2\theta\cos^2\theta+Q_{12}(\sin^4\theta+\cos^4\theta)$$
$$\bar{Q}_{22}=Q_{11}\sin^4\theta+2(Q_{12}+2Q_{66})\sin^2\theta\cos^2\theta+Q_{22}\cos^4\theta$$
$$\bar{Q}_{16}=(Q_{11}-Q_{12}-2Q_{66})\sin\theta\cos^3\theta+(Q_{12}-Q_{22}+2Q_{66})\sin^3\theta\cos\theta$$
$$\bar{Q}_{26}=(Q_{11}-Q_{12}-2Q_{66})\sin^3\theta\cos\theta+(Q_{12}-Q_{22}+2Q_{66})\sin\theta\cos^3\theta$$
$$\bar{Q}_{66}=(Q_{11}+Q_{22}-2Q_{12}-2Q_{66})\sin^2\theta\cos^2\theta+Q_{66}(\sin^4\theta+\cos^4\theta)$$

The bending stiffness matrix $[D]$ is defined as follows:

$$D_{ij}=\sum_{k=1}^{n}\int_{z_{k-1}}^{z_k}(\bar{Q}_{ij})_k\,z^2dz,\ i,j=1,2,6$$

(6)

In the above equation, $k$ and $n$ represent the layer number and the total number of layers, respectively. The potential and kinetic energies are obtained from Equations (7) and (8), respectively.

| | |
|---|---|
| $$U=\frac{1}{2}\int_{-h/2}^{h/2}\int_{-b/2}^{b/2}\int_{-a/2}^{a/2}(\sigma_{xx}\varepsilon_{xx}+\sigma_{yy}\varepsilon_{yy}+\sigma_{xy}\varepsilon_{xy})dxdydz$$ | (7) |
| $$T=\frac{\rho h}{2}\int_{-b/2}^{b/2}\int_{-a/2}^{a/2}\left(\frac{\partial^2 w}{\partial t^2}\right)^2 dxdy$$ | (8) |

By substituting the potential and kinetic energies into Lagrange's equation, the stiffness and mass matrices of the metallic and composite regions of the hybrid plate are obtained as follows:

| | |
|---|---|
| $$K_{metal}=\sum_{i=1}^{M}\sum_{j=1}^{N}\sum_{m=1}^{M}\sum_{n=1}^{N}\left\{\int_{-b/2}^{Y_{mc}}\int_{-a/2}^{a/2}D_m\begin{bmatrix}\left(X_{i,xx}X_{m,xx}Y_jY_n\right)\\+\left(X_iX_mY_{j,yy}Y_{n,yy}\right)+\\\nu\begin{pmatrix}X_{i,xx}X_mY_jY_{n,yy}\\+X_iX_{m,xx}Y_{j,yy}Y_n\end{pmatrix}\\+2(1-\nu)\left(X_{i,x}X_{m,x}Y_{j,y}Y_{n,y}\right)\end{bmatrix}dxdy\right\}$$ | (9) |
| $$M_{metal}=\sum_{i=1}^{M}\sum_{j=1}^{N}\sum_{m=1}^{M}\sum_{n=1}^{N}\left\{\int_{-b/2}^{Y_{mc}}\int_{-a/2}^{a/2}\rho_m h\left[X_iX_mY_jY_n\right]dxdy\right\}$$ | (10) |
| $$K_{composite}=\sum_{i=1}^{M}\sum_{j=1}^{N}\sum_{m=1}^{M}\sum_{n=1}^{N}\int_{Y_{mc}}^{b/2}\int_{-a/2}^{a/2}\begin{bmatrix}D_{11}\left(X_{i,xx}X_{m,xx}Y_jY_n\right)+D_{22}\left(X_iX_mY_{j,yy}Y_{n,yy}\right)+\\D_{12}\left(\left(X_{i,xx}X_mY_jY_{n,yy}+X_iX_{m,xx}Y_{j,yy}Y_n\right)\right)\\+4D_{66}\left(X_{i,x}X_{m,x}Y_{j,y}Y_{n,y}\right)+\\2D_{16}\left(X_i'X_m''Y_j'Y_n+X_i''X_m'Y_jY_n'\right)+\\2D_{26}\left(X_i'X_mY_j'Y_n''+X_iX_m'Y_j''Y_n'\right)\end{bmatrix}dxdy$$ | (11) |
| $$M_{composite}=\sum_{i=1}^{M}\sum_{j=1}^{N}\sum_{m=1}^{M}\sum_{n=1}^{N}\int_{Y_{mc}}^{b/2}\int_{-a/2}^{a/2}\rho_c h\left[X_iX_mY_jY_n\right]dxdy$$ | (12) |

In Equations (10) and (12), $\rho_m$ and $\rho_c$ represent the densities of the metallic and composite regions, respectively, and $D_m$ in Equation (9) is the bending stiffness of the metallic region, which is obtained from Equation (13).

| | |
|---|---|
| $D_m = \frac{(Eh^3)}{12(1-v^2)}$ | (13) |

Since the structure considered in this research is a wing, a cantilever boundary condition is applied, and the assumed-modes method is employed to obtain an approximate solution. In this method, a set of functions satisfying the geometric boundary conditions is assumed to represent the vibration modes of the plate. Accordingly, the transverse displacement of the plate is described using the following series expansion:

| | |
|---|---|
| $W(x,y,t) = \sum_{i=1}^{M}\sum_{j=1}^{N} a_{ij}(t) w_{ij}(x,y)$ | (14) |

In the above equation, $a_{ij}(t)$ is the generalized coordinate and \$w_{ij}(x,y)\$ is the mode shape function, defined as follows:

$$w_{ij}(x,y) = X_i(x)Y_j(y)$$

where Equations (15) and (16) are used for the x-direction (free–free) and the y-direction (clamped–free), respectively, in square plates with $a = b = 2\ m$.

| | |
|---|---|
| $X_i = \frac{1}{2^i\, i!} \frac{d^i}{dx^i} \left( \left( \frac{x+1}{2} \right)^2 - 1 \right)^i, \quad i = 0, 1, 2, \ldots$ | (15) |

| | |
|---|---|
| $Y_j = \left( \frac{y+1}{2} \right)^{j+1}, \quad j = 1, 2, 3, \ldots$ | (16) |

Figure 2 shows a schematic of a cantilever square hybrid plate together with the coordinate system used in the formulation.

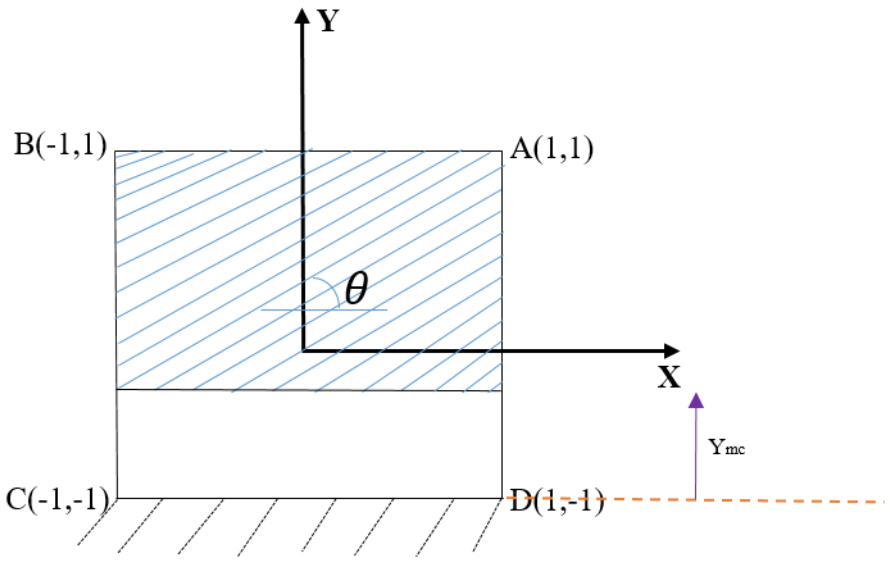



**Fig. 2.** A square hybrid plate.

By substituting Equations (15) and (16) into Equations (9) to (12), the stiffness and mass matrices of the metallic and composite regions are obtained. Since the trapezoidal wing is modeled in this research as a hybrid metal–composite structure, and assuming a perfectly bonded interface, such that the transverse displacement and its slope are continuous across the metal–composite junction, the stiffness and mass matrices of the hybrid structure are obtained as follows:

| | |
|---|---|
| $K = K_{metal} + K_{composite}$ | (17) |
| $M = M_{metal} + M_{composite}$ | (18) |

The equations for non-rectangular geometries are derived by means of a one-to-one mapping from the x–y plane to the u–v plane, defined by the following relations:

| | |
|---|---|
| $\begin{cases} x = \sum_{i=1}^{4} N_i(u,v)\, x_i \\ y = \sum_{i=1}^{4} N_i(u,v)\, y_i \end{cases}$ | (19) |

where $N_i$ is the mapping function, defined as follows:

$$N_i(u,v) = \frac{1}{4}(1+u_i u)(1+v_i v), i = 1,2,3,4$$

The elements of the Jacobian matrix are calculated as follows:

| | |
|---|---|
| $J = \sum_{i=1}^{4} \begin{bmatrix} \frac{\partial N_i}{\partial u} \\ \frac{\partial N_i}{\partial v} \end{bmatrix} \begin{bmatrix} x_i & y_i \end{bmatrix}$ | (20) |

finally:

| | |
|---|---|
| $dA = \lvert J \rvert dudv$ | (21) |

where $|J|$ is the determinant of the Jacobian matrix.

Thus, by defining $[\Gamma] = [J]^{-1}$, the derivatives of a quantity with respect to the x–y coordinates can be expressed as follows:

| | |
|---|---|
| $\begin{cases} \frac{\partial}{\partial x} = \Gamma_{11}\frac{\partial}{\partial u} + \Gamma_{12}\frac{\partial}{\partial v} \\ \frac{\partial}{\partial y} = \Gamma_{21}\frac{\partial}{\partial u} + \Gamma_{22}\frac{\partial}{\partial v} \end{cases}$ | (22) |

Noting that $w(x, y) = w(u, v)$, and substituting Equations (19) to (22) into Equations (17) and (18), the stiffness and mass matrices of a non-rectangular hybrid wing are obtained.

It should be noted that the structure in the vicinity of the interface can exhibit significant nonlinearity and discontinuities, owing to factors such as the stiffness mismatch between the metal and the composite. However, these effects are neglected in the present research.

**2.2 Aerodynamic Model**

In this study, piston theory is used for the aerodynamic model in the supersonic regime, which provides a linear relationship between the pressure perturbation and the surface velocity in the flow direction. The airfoil is assumed to be thin and the angle of attack small, so that the flow can be linearized. The effects of viscosity are neglected and the airflow over the wing is treated as a potential flow. The lift force and the aerodynamic moment are obtained by integrating the pressure field. In supersonic flow, the differential pressure is obtained from piston theory according to the following equation [18]:

| | |
|---|---|
| $\Delta p = -\xi \frac{\partial W}{\partial x} - \mu \frac{\partial W}{\partial t}$ | (23) |

where

$$\xi = \frac{\rho_\infty U^2{}_\infty}{\sqrt{M_\infty{}^2 - 1}}, \mu = \frac{\rho_\infty U_\infty \left(M_\infty{}^2 - 2\right)}{\left(M_\infty{}^2 - 1\right)^{\frac{3}{2}}}$$

In the above equations, $M_\infty$ is the freestream Mach number, defined as follows:

| | |
|---|---|
| $M_\infty = \frac{U_\infty}{a}$ | (24) |

where $U_\infty$ is the freestream velocity and $a$ is the speed of sound.

### 2.3 p-Method for Flutter Analysis

The p-method is a numerical technique used for flutter analysis in supersonic flows, in which the aerodynamic forces are described by linear potential flow theory or piston theory. The method aims to determine the critical speed, or dynamic pressure, at which flutter occurs, and requires the solution of an eigenvalue problem whose eigenvalues represent the frequencies and damping of the structure. It exploits the fact that, at the onset of flutter, the system is neutrally stable, that is, the real part of one of the eigenvalues of the characteristic equation vanishes, indicating neither growth nor decay of the oscillation amplitude.

The matrix form of the aeroelastic equation of motion is given as follows:

| | |
|---|---|
| $[M]\{\ddot{\vec{q}}\}+[K]\{\vec{q}\}=\{Q\}$ | (25) |

where $[Q]$ is obtained from the following equation:

| | |
|---|---|
| $q_w=\left\{\int_A \Delta p W dA\right\}$ | (26) |

In the above equation, $\Delta p$ is obtained from piston theory. Thus, the aerodynamic force vector is calculated as follows:

| | |
|---|---|
| $\{Q\}=\left[\bar{Q}\right]\{\vec{q}\}$<br>$\left[\bar{Q}\right]=\left[\int_{-1}^{1}\int_{-1}^{1}\begin{Bmatrix}-\xi\left(\Gamma_{11}u_{i,u}v_j+\Gamma_{12}u_i v_{j,v}\right)u_m v_n\\ -p\mu u_i v_j u_m v_n\end{Bmatrix}\lvert J\rvert dudv\right]$ | (27) |

Noting that:

| | |
|---|---|
| $\vec{q} = \vec{\bar{q}} e^{pt} \rightarrow \begin{cases} \dot{\vec{q}} = p \times \vec{\bar{q}} e^{pt} \\ \ddot{\vec{q}} = p^2 \times \vec{\bar{q}} e^{pt} \end{cases}$ | (28) |

By substituting Equations (27) and (28) into Equation (25), the equation of motion becomes:

| | |
|---|---|
| $P^2 [M]\{\vec{q}\} + [K]\{\vec{q}\} = [\bar{Q}]\{\vec{q}\}$ | (29) |

By solving the eigenvalue problem, the values of $p$ are obtained [18].

The optimization problem consists in finding the stacking sequence that maximizes the flutter speed of trapezoidal hybrid metal–composite swept wings. It should be noted that the symmetry requirement is easily enforced by optimizing only one half of the laminate and obtaining the other half from the symmetry condition. The optimal design problem can be stated as follows:

| | |
|---|---|
| $\begin{cases} \text{Find :} \quad \theta = (\theta_1, \theta_2, \theta_3, \theta_4) \\ \text{Maximize : f}(\theta) \quad \text{Flutter Speed} \\ \text{Subject to :} \; -90 \le \theta \le 90 \end{cases}$ | (30) |

The optimal stacking sequences are searched for using the EA-PSO algorithm, and the maximum flutter speed is obtained for different geometric parameters, namely the metal span fraction, aspect ratio, taper ratio and sweep angle.

### 3. Elitist Adaptive Particle Swarm Optimization Algorithm

In this research, an elitist adaptive particle swarm optimization (EA-PSO) algorithm is employed for flutter optimization. Particle swarm optimization (PSO) is an optimization algorithm inspired

by the social behavior of flocking birds or schooling fish. In this algorithm, a group of particles, each representing a potential solution, explores the solution space in order to find an optimal or near-optimal solution. The algorithm is initialized with a group of randomly distributed particles, and each particle then evaluates the objective function at its current position in the search space. Each particle has a position vector that represents its current location in the search space, and a velocity vector that determines the direction and magnitude of its movement. Each particle retains the best position it has found so far, known as the personal best ( $p_{best}$ ), while the best position found by the entire swarm is known as the global best ( $g_{best}$ ). Once all the particles have been updated, one iteration of the algorithm is completed, and this process is repeated until the stopping criterion is met and the optimal solution is obtained.

In the elitist version of the PSO algorithm, in contrast to the basic version, the previous positions of the particles are not discarded once the new positions have been determined. Instead, they are compared with the new positions, and the best positions, referred to as the elites, are used to determine $p_{best}$ and $g_{best}$. As a result, the convergence rate of the algorithm is increased by applying the elitist strategy.

In this algorithm, the position and velocity of each particle in the swarm are updated using the following equations [19]:

| | |
|---|---|
| $X_k(i+1) = X_k(i) + V_k(i+1)$ | (31) |
| $V_k(i+1) = \omega V_k(i) + c_1 r_1 \left( p_{best}^k(i) - X_k(i) \right) + c_2 r_2 \left( g_{best}(i) - X_k(i) \right)$ | (32) |

where the superscript $k$ denotes the particle and the subscript $i$ denotes the iteration number; $X$ and $V$ are the position and the velocity of the particle, respectively; $c_1$ and $c_2$ are the acceleration

coefficients that control the influence of $p_{best}$ and $g_{best}$; $r_1$ and $r_2$ are random numbers uniformly distributed in $[-1,1]$, which introduce stochastic behavior into the algorithm; and $w$ is the inertia weight, which balances exploration and exploitation. In the present work, $c_1 = c_2 = 1$ are adopted, as these values yield better optimal results in fewer iterations [20].

One of the most important parameters of this algorithm is the inertia weight $w$, which plays a crucial role in the performance of the algorithm by balancing exploration and exploitation. Exploration refers to creating diversity in the population in order to survey the entire search space, whereas exploitation refers to reducing this diversity in order to refine the search around the best members of the population in the later iterations. The inertia weight always takes a value between 0 and 1. It is preferable to vary this value throughout the optimization process, since a small value leads to exploitation alone and a large value leads to exploration alone. Therefore, adjusting the inertia weight during the solution process plays a significant role in improving both the convergence time and the quality of the solution. In this research, a new adaptive inertia-weight function, given in Equation (37), is proposed for this purpose.

| | |
|---|---|
| $\omega = 1 - x^{\beta}$ | (33) |

In the above equation, $\beta$ is a parameter controlling the rate of decay of the inertia weight, taken as $\beta = 0.4$ in the present work, and $x$ is defined as follows:

| | |
|---|---|
| $x = \frac{fit_{\min}}{fit_{\max}}$ | (34) |

Therefore, as the solutions gradually converge, the inertia weight approaches zero, which reduces the diversity among the particles and accelerates the convergence of the algorithm. In the adaptive version, the tendency of the inertia weight towards zero can itself be used as the stopping criterion of the algorithm. The flowchart of the EA-PSO algorithm is presented in Figure 3.

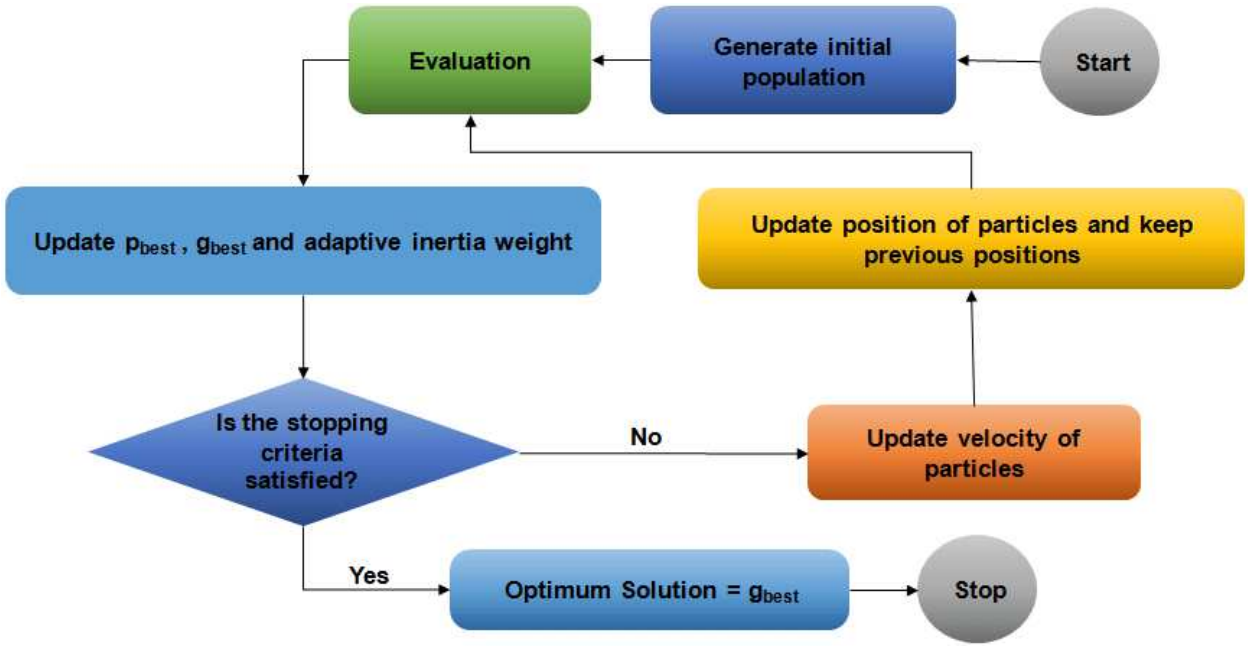



**Fig. 3.** Flowchart of EA-PSO algorithm

## 4. Numerical results and discussions

In the present study, the flutter speed of trapezoidal hybrid metal–composite swept wings is maximized for different metal span fractions, aspect ratios, taper ratios and sweep angles. In all the structures investigated, aluminum 2024 alloy is used for the metallic section and graphite/epoxy AS/3501 is used for the layers of the composite section. The mechanical properties of the aluminum and the composite layers are listed below [21, 22]:

Aluminum: $E = 73$ GPa, $\nu = 0.3$ , $\rho = 2800$ kg/m³

Composite layers: $E_1 = 138\,\text{GPa},\ E_2 = 8.96\,\text{GPa},\ G_{12} = 7.1\,\text{GPa},\ \nu_{12} = 0.3,\ \rho = 1600\,\text{kg/m}^3$

All the composite laminae are assumed to have the same thickness. The specifications of the investigated laminates are listed in Table 1.

**Table 1.** Geometric characteristics of the compared structures

| *Case* | *Sweep angle* | *Taper Ratio* | $C_r$ | $Span/C_r$ | $h$ |
|---|---|---|---|---|---|
| *a* | $0^\circ$ | *0.70* | *2m* | *1* | *0.020m* |
| *b* | $0^\circ$ | *0.80* | *2m* | *1* | *0.020m* |
| *c* | $0^\circ$ | *0.90* | *2m* | *1* | *0.020m* |
| *d* | $0^\circ$ | *0.50* | *2m* | *1* | *0.018m* |
| *e* | $0^\circ$ | *0.50* | *2m* | *1.5* | *0.018m* |
| *f* | $0^\circ$ | *0.50* | *2m* | *1.75* | *0.018m* |
| *g* | $30^\circ$ | *0.20* | *2m* | *0.8660* | *0.012m* |
| *h* | $40^\circ$ | *0.20* | *2m* | *0.7660* | *0.012m* |
| *i* | $50^\circ$ | *0.20* | *2m* | *0.6428* | *0.012m* |
| *f* | $0^\circ$ | *1* | *2m* | *1* | *0.024m* |

To demonstrate the superiority of the elitist adaptive version of the particle swarm optimization algorithm over the basic version, the performance of both algorithms is compared in Figure 4 for four 8-layer laminates with the layup of $[\theta_1 / \theta_2 / \theta_3 / \theta_4]_s$.

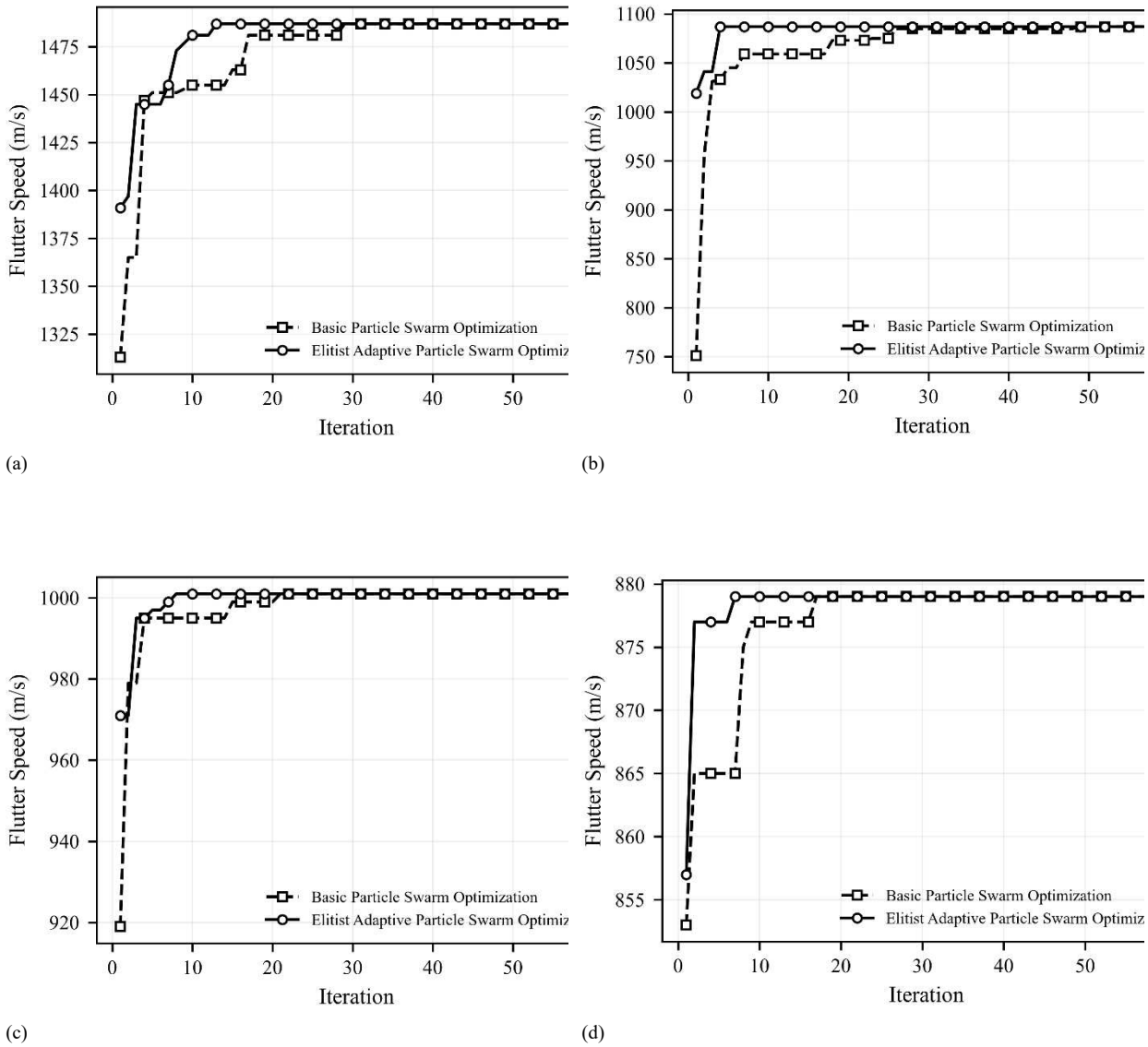



**Fig. 4.** Comparison of the EA-PSO and PSO results: (a) case *d*, (b) case *e*, (c) case *h*, (d) case *b*.

Figure 4 demonstrates that, for the 8-layer symmetric plates, the EA-PSO algorithm converges in an average of 10 iterations, whereas the basic PSO algorithm requires an average of 30 iterations to converge. This comparison indicates that, the EA-PSO algorithm has a faster convergence rate than the basic version. This is due to the elitist approach and the use of an adaptive strategy in the algorithm, which improves the quality of the results at each step compared with the previous one.

To validate the structural model, the present analytical model is applied to an 8-layer symmetric hybrid plate with a cantilever boundary condition and a metal span fraction of $\lambda_m = 0.5$, using the geometric characteristics of case (f). The results are compared with those obtained from ABAQUS and are presented in Table 2.

**Table 2.** Structural model validation.

| Analysis method | $\omega_1(HZ)$ | $\omega_2(HZ)$ | $\omega_3(HZ)$ | $\omega_4(HZ)$ |
|---|---|---|---|---|
| ABAQUS software | 6.3160 | 13.452 | 28.395 | 31.481 |
| Present study | 6.4026 | 13.839 | 28.938 | 32.711 |
| Percentage of difference | 1.3711 | 2.8769 | 1.9123 | 3.9071 |

The comparison of the results demonstrates the efficiency and accuracy of the present method. In addition, in a previous work [5], the flutter of a hybrid metal–composite trapezoidal wing in supersonic flow was validated against the results reported by Nakai et al. [23]. The validated code is therefore employed for the flutter optimization of the hybrid metal–composite trapezoidal wing. In the following, the flutter optimization of the hybrid trapezoidal wing is presented for different aspect ratios, taper ratios, sweep angles and metal span fractions. The optimization process converged, on average, within 10 iterations using a swarm of 70 particles, and a predefined threshold for the inertia weight was adopted as the stopping criterion of the algorithm. The optimal stacking sequences and the corresponding maximum flutter speeds of the hybrid trapezoidal wing for different aspect ratios are presented in Table 3.

**Table 3.** Optimal stacking sequences and flutter speed for different aspect ratios.

| *Case* | $\lambda_m$ | *0.25* | | *0.35* | | *0.5* | |
|---|---|---|---|---|---|---|---|
| | *Span/$C_r$* | *Optimum Ply angles* | $V_{F_{Opt}}(m/s)$ | *Optimum Ply angles* | $V_{F_{Opt}}(m/s)$ | *Optimum Ply angles* | $V_{F_{Opt}}(m/s)$ |
| *d* | 1 | $[20/-65/20/19]_s$ | 1487 | $[12/12/-71/-74]_s$ | 1457 | $[5/2/11/78]_s$ | 1461 |
| *e* | 1.5 | $[11/2/-2/37]_s$ | 1087 | $[2/-10/-10/57]_s$ | 1095 | $[-10/-6/-12/38]_s$ | 1347 |
| *f* | 1.75 | $[1/-2/-21/9]_s$ | 1019 | $[0/-13/1/6]_s$ | 1069 | [-2/-25/-19/14]s | 1199 |

The optimal flutter speeds for various aspect ratios and metal span fractions are compared with the flutter speeds of three other layups in Fig. 5. The comparison demonstrates that, for all the metal span fractions considered, the present optimal solutions yield higher flutter speeds than the wings with the other layups.

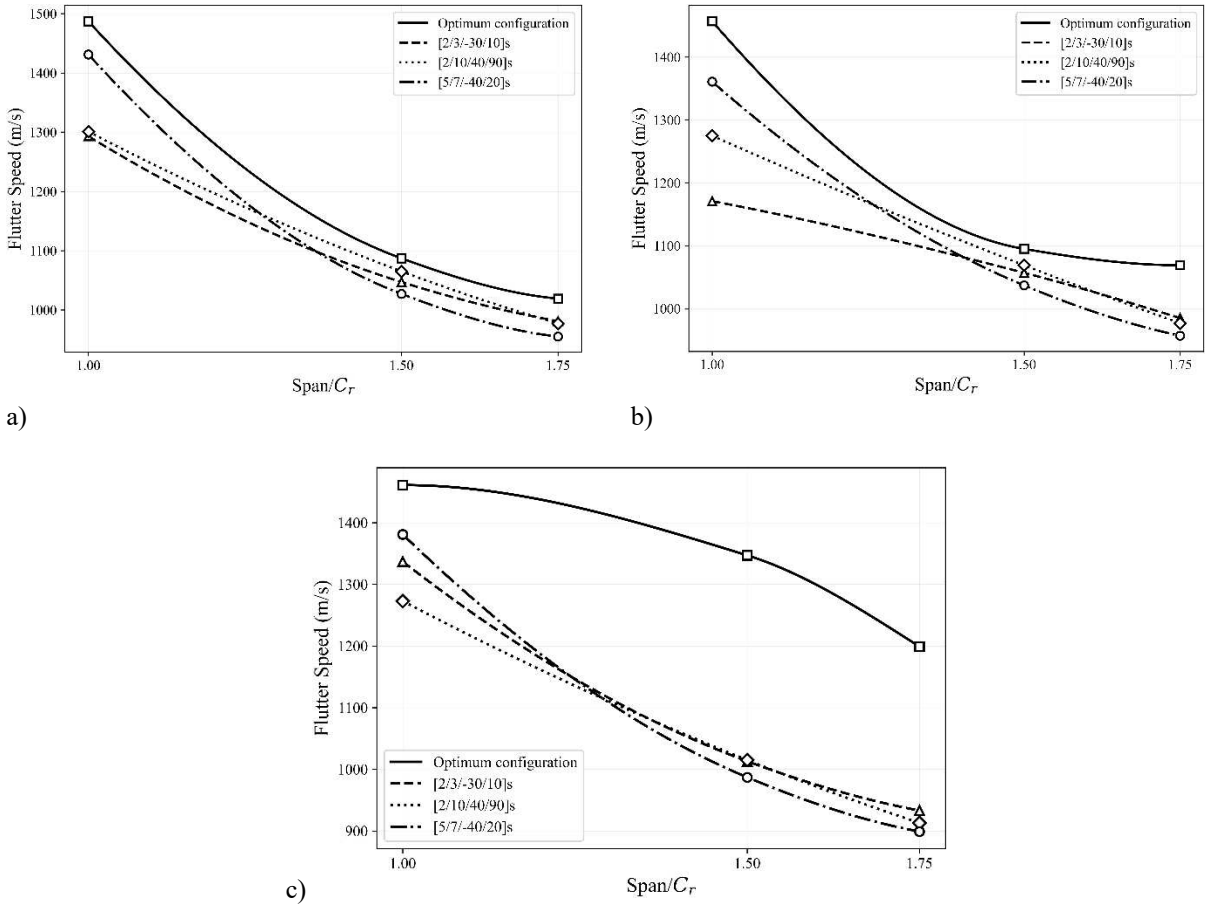



**Fig 5.** Comparison of the optimal flutter speeds with the flutter speed of three other lay-ups for various aspect ratios and metal span fraction: (a) 0.25, (b) 0.35, (c) 0.50.

The obtained results show the good performance of the EA-PSO algorithm and its ability to provide high-quality solutions. In addition, the results show that the optimal layer angles do not follow a particular trend as the aspect ratio increases. However, as the aspect ratio increases, the optimal flutter speed decreases. This behaviour is attributed to the simultaneous influence of the structural stiffness and the shape of the coupled modes on the flutter speed: as the aspect ratio increases, the structural stiffness decreases in addition to the adverse effect of the coupled mode shapes, and consequently flutter occurs at a lower speed.

The maximum flutter speeds and the optimum fibre orientations of the hybrid trapezoidal wing for different sweep angles are given in Table 4.

Similarly, the optimal flutter speeds for various sweep angles and metal span fractions are compared with the flutter speeds of three other layups in Fig. 6. It can be observed from the results that the EA-PSO algorithm successfully predicts the maximum flutter speed and the optimal stacking sequences.

**Table 4.** Optimal stacking sequences and flutter speed for different sweep angles.

| *Case* | $\lambda_m$ | *0.25* | | *0.50* | | *0.75* | |
|---|---|---|---|---|---|---|---|
| | *Sweeep Angle* | *Optimum Ply angles* | $V_{F_{Opt}}(m/s)$ | *Optimum Ply angles* | $V_{F_{Opt}}(m/s)$ | *Optimum Ply angles* | $V_{F_{Opt}}(m/s)$ |
| *g* | 30° | $[17/8/4/19]_s$ | 1059 | $[14/8/6/9]_s$ | 1079 | $[1/-39/-18/-21]_s$ | 919 |
| *h* | 40° | $[0/5/-45/-44]_s$ | 1001 | $[-4/-5/-55/4]_s$ | 1049 | $[1/-53/-7/-19]_s$ | 1029 |
| *i* | 50° | $[-60/-53/-50/-22]_s$ | 1339 | $[-56/-9/-1/12]_s$ | 1309 | $[-5/-74/-5/90]_s$ | 1409 |

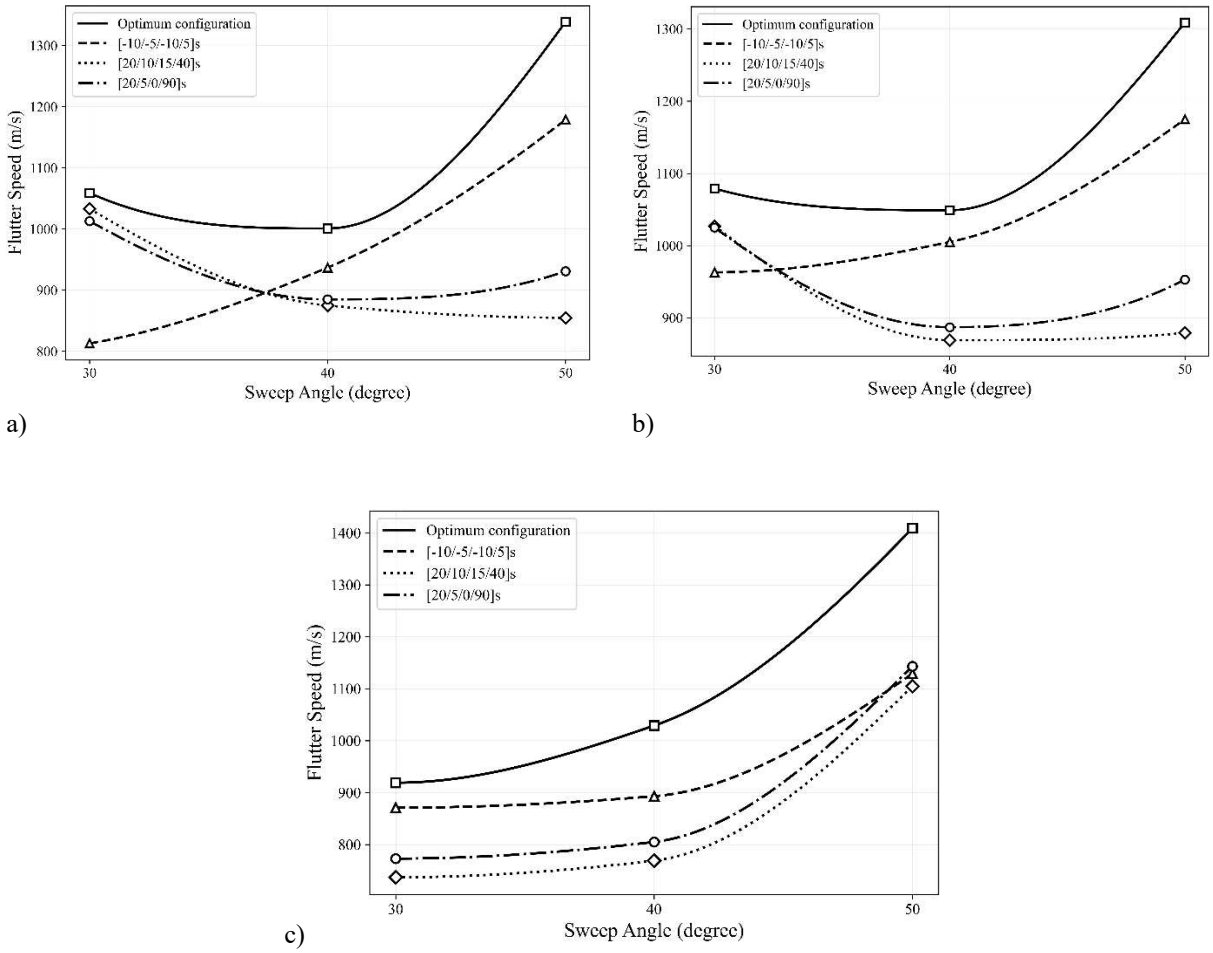



**Fig 6.** Comparison of the optimal flutter speeds with the flutter speed of three other lay-ups for various sweep angles and metal span fraction: (a) 0.25, (b) 0.50, (c) 0.75.

The obtained results show the good efficiency of the present algorithm in predicting the optimal flutter speed. The results also show that the optimal flutter speed does not vary monotonically with the sweep angle. The reason for this behaviour is that, in addition to the structural stiffness, the shape of the coupled modes also influences the flutter speed. When its reducing effect outweighs the increasing effect arising from the higher structural stiffness, the flutter speed decreases.

The optimal ply angles and the corresponding flutter speeds for various taper ratios are also presented in Table 5.

**Table 5.** Optimal stacking sequences and flutter speed for different taper ratios.

| Case | $\lambda_m$ | 0.25 | | 0.50 | | 0.75 | |
|---|---|---|---|---|---|---|---|
| | Taper ratio | Optimum Ply angles | $V_{F_{Opt}}(m/s)$ | Optimum Ply angles | $V_{F_{Opt}}(m/s)$ | Optimum Ply angles | $V_{F_{Opt}}(m/s)$ |
| a | 0.70 | $[28/-62/24/24]_s$ | 1409 | $[24/-73/23/13]_s$ | 1261 | $[0/4/0/90]_s$ | 1099 |
| b | 0.80 | $[22/23/-66/-69]_s$ | 1193 | $[24/-73/26/31]_s$ | 1053 | $[9/10/-89/-87]_s$ | 879 |
| c | 0.90 | $[26/25/-67/-72]_s$ | 1013 | $[26/-67/26/15]_s$ | 881 | $[14/16/-82/-88]_s$ | 709 |

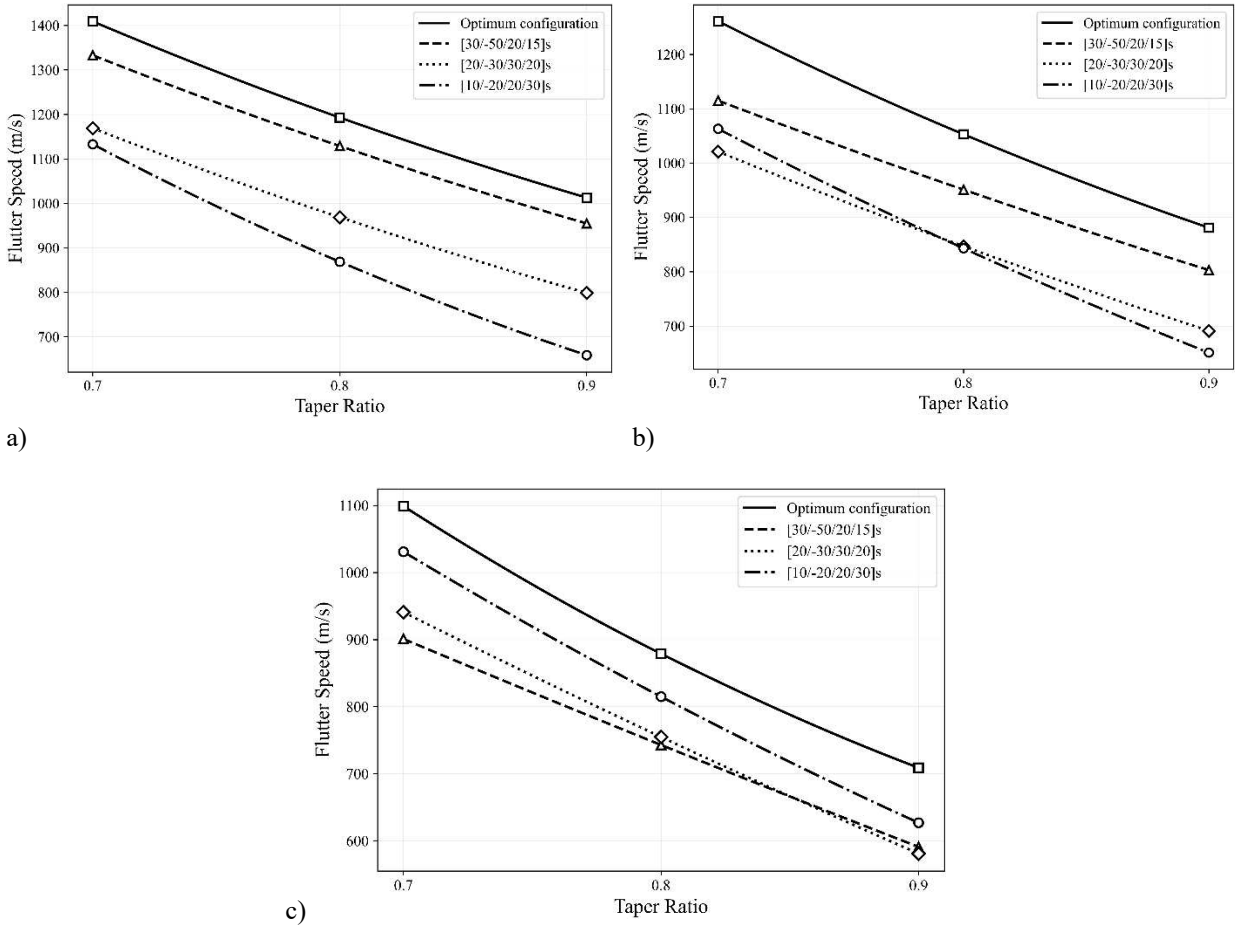



**Fig 7.** Comparison of the optimal flutter speeds with the flutter speed of three other lay-ups for various taper ratios and metal span fraction: (a) 0.25, (b) 0.50, (c) 75.

In another similar investigation, the optimal flutter speeds for various taper ratios and metal span fractions are compared with the flutter speeds of three other layups in Fig. 7. The results show that the EA-PSO algorithm is successful in determining the optimal flutter speed and the corresponding stacking sequences. The results also indicate that the optimal ply angles do not follow a certain

trend as the taper ratio increases from 0.70 to 0.90, whereas the optimal flutter speed decreases. This is attributed to the adverse effects of both the coupled mode shapes and the structural stiffness. Overall, the results show that a structural designer who is unaware of the influence of the ply angles on the flutter speed may select a stacking sequence that is far from the optimal one.

## 5. Conclusions

In this research, the flutter speed of swept trapezoidal hybrid metal–composite wings was optimized using an elitist adaptive particle swarm optimization algorithm with an improved inertia-weight function. The results obtained for various geometries demonstrated the good efficiency of the present algorithm in predicting the optimal flutter speed, and showed that, as the sweep angle increases, neither the optimal ply angles nor the maximum flutter speed follows a monotonic trend. This is due to the simultaneous influence of the structural stiffness and the shape of the coupled modes on the flutter speed: when the adverse effect of the coupled modes outweighs the beneficial effect of the increased structural stiffness, the flutter speed decreases, and vice versa.

Furthermore, the results showed that the optimal ply angles do not follow a certain trend as the aspect ratio or the taper ratio increases, whereas the optimal flutter speed decreases. This is because an increase in either ratio causes both the coupled mode shapes and the structural stiffness to act adversely, thereby lowering the flutter speed.

An investigation of the effect of the metal span fraction for different geometries showed that increasing the metal span fraction does not necessarily decrease or increase the maximum flutter speed, since the structural stiffness and the coupled mode shapes are governed by the combined effects of the geometry, the fibre angles and the metal span fraction. Consequently, the optimal ply

angles and the maximum flutter speed are specific to each geometry. Finally, the results showed that the proposed inertia-weight function is effective and may be adopted in future studies.

**References**

[1] J.W. Sawyer, Flutter of Laminated Plates in Supersonic Flow, Ph.D. dissertation, Virginia Polytechnic Institute and State University, Blacksburg, VA, 1975. http://hdl.handle.net/10919/88687.

T.A. Weisshaar, J.D. Bohlmann, Supersonic flutter of aeroelastically tailored oblique wings, J. Aircr. 26 (1) (1989) 75–83. https://doi.org/10.2514/3.45725.

[3] J. Cho, Y. Chang, Supersonic flutter analysis of wings using an unsteady 3D panel method, Comput. Fluids 30 (2) (2001) 237–256. https://doi.org/10.1016/S0045-7930(00)00010-4.

[4] W.W. Zhang, Z.Y. Ye, C. Zhang, F. Liu, Supersonic flutter analysis based on a local piston theory, AIAA J. 47 (10) (2009) 2321–2328. https://doi.org/10.2514/1.37750.

[5] H. Golparvar, S. Irani, M. Mousavi Sani, Experimental investigation of linear and nonlinear aeroelastic behavior of a cropped delta wing with store in low subsonic flow, J. Braz. Soc. Mech. Sci. Eng. 38 (4) (2016) 1113–1130. https://doi.org/10.1007/s40430-015-0436-z.

[6] S. Shokrollahi, S. Shafaghat, Flutter analysis of hybrid metal-composite low aspect ratio trapezoidal wings in supersonic flow, Chin. J. Aeronaut. 30 (1) (2017) 196–203. https://doi.org/10.1016/j.cja.2016.12.016.

[7] S. Guo, W. Cheng, D. Cui, Optimization of composite wing structures for maximum flutter speed, in: 46th AIAA/ASME/ASCE/AHS/ASC Structures, Structural Dynamics and Materials Conference, Austin, TX, 2005, AIAA Paper 2005-2132. https://doi.org/10.2514/6.2005-2132.

[8] Z.G. Song, F.M. Li, Optimal locations of piezoelectric actuators and sensors for supersonic flutter control of composite laminated panels, J. Vib. Control 20 (14) (2014) 2118–2132. https://doi.org/10.1177/1077546313480538.

[9] K. Torabi, H. Afshari, Optimization of flutter boundaries of cantilevered trapezoidal functionally graded sandwich plates, J. Sandw. Struct. Mater. 21 (2) (2019) 503–531. https://doi.org/10.1177/1099636217697492.

[10] T.A.M. Guimarães, S.G.P. Castro, C.E.S. Cesnik, D.A. Rade, Supersonic flutter and buckling optimization of tow-steered composite plates, AIAA J. 57 (1) (2019) 397–407. https://doi.org/10.2514/1.J057282.

[11] M. Ghalandari, I. Mahariq, F. Ghadak, O. Accouche, F. Jarad, Aeroelastic optimization of the high aspect ratio wing with aileron, Comput. Mater. Contin. 70 (3) (2022) 5569–5581. https://doi.org/10.32604/cmc.2022.020884.

[12] M.R. Amoozgar, S.A. Fazelzadeh, H. Haddad Khodaparast, M.I. Friswell, J.E. Cooper, Aeroelastic stability analysis of aircraft wings with initial curvature, Aerosp. Sci. Technol. 107 (2020) 106241. https://doi.org/10.1016/j.ast.2020.106241.

[13] E. Zafari, M.M. Jalili, A. Mazidi, Analytical nonlinear flutter and sensitivity analysis of aircraft wings subjected to a transverse follower force, Proc. Inst. Mech. Eng. Part G J. Aerosp. Eng. 233 (4) (2019) 1503–1515. https://doi.org/10.1177/0954410017754171.

[14] H. Guo, M. Li, K.K. Żur, J. Yuan, X. Wu, Flutter of carbon-based nanohybrid composite panels, Thin-Walled Struct. 188 (2023) 110828. https://doi.org/10.1016/j.tws.2023.110828.

[15] P. Timoshenko, J.N. Goodier, Theory of Elasticity, 2nd ed., McGraw-Hill, New York, 1951.

[16] S.S. Rao, Vibration of Continuous Systems, John Wiley & Sons, Hoboken, NJ, 2007. ISBN 978-0-471-77171-5.

[17] J.N. Reddy, Mechanics of Laminated Composite Plates and Shells: Theory and Analysis, 2nd ed., CRC Press, Boca Raton, FL, 2004. ISBN 0-8493-I592-1

[18] E.H. Dowell, H.C. Curtiss Jr. GR, D.A. Peters, et al, A Modern Course in Aeroelasticity, 4th ed., Solid Mechanics and Its Applications, vol. 116, Kluwer Academic Publishers, Dordrecht, 2004. https://doi.org/10.1007/1-4020-2106-2.

[19] M. Jain, V. Saihjpal, N. Singh, S.B. Singh, An overview of variants and advancements of PSO algorithm, Appl. Sci. 12 (17) (2022) 8392. https://doi.org/10.3390/app12178392.

[20] H. Ghashochi Bargh, M.H. Sadr, Stacking sequence optimization of composite plates for maximum fundamental frequency using particle swarm optimization algorithm, Meccanica 47 (3) (2012) 719–730. https://doi.org/10.1007/s11012-011-9482-5.

[21] S.W. Tsai, H.T. Hahn, Introduction to Composite Materials, Technomic Publishing Co., Westport, CT, 1980. ISBN 0-87762-288-4.

[22] F.P. Beer, E.R. Johnston Jr., J.T. DeWolf, D.F. Mazurek, Mechanics of Materials, 5th ed., McGraw-Hill Higher Education, Boston, 2009. ISBN 978-0-07-352938-7.

[23] E. Nakai, T. Takagi, K. Isogai, Results of supersonic flutter characteristics of low aspect-ratio flat-plate surfaces, AIAA J. 5 (9) (1967) 1715–1717. https://doi.org/10.2514/3.4290.